Chemical Engineering Science 288 (2024) 119780

Contents lists available at ScienceDirect

Chemical Engineering Science

journal homepage: www.elsevier.com/locate/ces

A new model-aided approach for the design of packed columns for CO_2 absorption in aqueous NH_3 solutions

Federico Atzori [a,d,*], Francesco Barzagli [b], Suzhou Dai [b,c], Alessandro Concas [a,d,*], Giacomo Cao [a,d,e]

[a] Interdepartmental Center of Environmental Science and Engineering (CINSA), University of Cagliari, Via San Giorgio 12 09124, Cagliari, Italy
[b] National Research Council (CNR), ICCOM Institute, via Madonna del Piano 10 50019, Sesto F.no, Florence, Italy
[c] School of Energy and Environment, Southeast University, Nanjing 210096, China
[d] Department of Mechanical, Chemical and Materials Engineering, University of Cagliari, Piazza d'Armi 09123 Cagliari, Italy
[e] Center for Advanced Studies, Research and Development in Sardinia (CRS4), Loc. Piscina Manna, Building 1 09050 Pula CA, Italy

ARTICLE INFO

Keywords:
CO_2 absorption
NH_3 sorbent solution
Packed column
Design algorithm
Shooting method

ABSTRACT

A novel model-based approach to design packed beds for CO_2 absorption with NH_3 is proposed and experimentally validated. The two-film theory is adopted to model gas/liquid mass transfer while the thermodynamic equilibrium among ion species is considered in the liquid. Such strategy allows to simulate both CO_2 absorption and NH_3 evaporation, that represent the most important aspects to improve capture efficiency and process cost-effectiveness. The resulting ODEs system is a two boundary-value problem which is solved by means of the shooting method. The model is then exploited to develop a new algorithm that, based on the adopted operating conditions, evaluates the packed bed height as a function of the desired capture efficiency. The height calculated for different combinations of operating conditions is successfully compared with the real height of the experimental column, thus confirming the reliability of the developed tool which can be run with very low computational loads.

1. Introduction

According to the Emission Database for Global Atmospheric Research, global CO_2 emissions in 2020 decreased by 5.3 % as compared to 2019, mainly because of the COVID-19 pandemic (Crippa et al. (2022)). However, in 2021, global emissions bounced back almost to the level of 2019, thus reaching 37.9 Gt (Crippa et al. (2022)), and, according to the analysis from NOAA's Global Monitoring Lab, CO_2 atmospheric concentration reached a value of 419.31 ppm at the beginning of 2023 (NOAA, National Centers for Environmental Information, 2023). As a consequence, the ongoing and prospective challenge will be implementing appropriate methods to minimize greenhouse gas emissions.

Since power plants and chemical industries are the primary sources of CO_2 emissions, in recent years many studies have been conducted to develop different Carbon Capture and Storage (CCS) technologies to relief the environmental impact of such industries. Among the post-combustion CCS methods, that include adsorption processes, cryogenic capture, physical absorption and membrane separation, the one based on chemical absorption turns out to be the most accepted and reliable choice by the chemical, petrochemical, and other industries (Ochedi et al., 2021). With respect to physical absorption, where CO_2 is absorbed at high pressure and low temperature and solvent regeneration is achieved via heating, pressure reduction or both, the chemical absorption involves the usage of solvents capable to increase the solution capture capacity by exploiting the reactions taking place in the liquid phase between absorbed CO_2 and chemicals in the liquid. Since chemical absorption is not limited by low contaminant partial pressure, flue gas with CO_2 concentration less than 15 $\%_{vol}$ can be treated, thus dramatically reducing the pressurization energy (Ochedi et al., 2021). Therefore, one of the most significant challenges in the CO_2 capture process is to discover and develop chemical solvents with high CO_2 absorption capacity, low regeneration energy, low solvent degradation and equipment corrosion as well as low volatility to minimize make-up streams.

Nowadays, amines are the most used CO_2 chemical sorbents, with a long history in the petroleum and chemical industries. However, despite the large capture capacity, they show several drawbacks and limitations

* Corresponding authors at: Interdepartmental Center of Environmental Science and Engineering (CINSA), University of Cagliari, Via San Giorgio 12 09124, Cagliari, Italy (A. Concas)
E-mail addresses: federico.atzori@unica.it (F. Atzori), alessandro.concas@unica.it (A. Concas).

https://doi.org/10.1016/j.ces.2024.119780
Received 12 September 2023; Received in revised form 27 December 2023; Accepted 16 January 2024
Available online 19 January 2024

Nomenclature

a	Specific surface area of packed bed [m^2/m^3]
a_w	Wetted area per unit volume [m^2/m^3]
C	Concentration [mol/m^3]
$D_{i,G}$	Diffusivity of *i* in the gas phase [m^2/s]
$D_{i,L}$	Molecular diffusivity of *i* in the liquid phase [m^2/s]
$D_{CO2,H2O}$	Molecular diffusivity of CO_2 in pure water [m^2/s]
d_C	Internal diameter of the column [m]
d_p	Nominal diameter of the packing particle [m]
G	Gas molar flow rate [mol/s]
G_g	Gas mass flux [$kg/(m^2\ s)$]
g	Gravity acceleration = 9.80665 [m/s^2]
H	Henry constant [Pa m^3/mol]
Ha	Hatta number [-]
J	Molar flux through gas/liquid interface [$mol/(s\ m^2)$]
K_j	Equilibrium constant Tab. 3
$K_{i,G}$	Gas phase overall transfer coefficient [$mol/(m^2\ s\ Pa)$]
$k_{i,G}$	Gas phase local transfer coefficient [$mol/(m^2\ s\ Pa)$]
$k_{i,L}$	Liquid phase local transfer coefficient [m/s]
k_{app}	Apparent kinetic constant [1/s]
L	Liquid molar flow rate [mol/s]
L_g	Liquid mass flux [$kg/(m^2\ s)$]
MW	Molecular weight [g/mol]
P	Total pressure [Pa]
p	Partial pressure [Pa]
p*	Equilibrium partial pressure [Pa]
Q_G	Gas volumetric flow rate [m^3/s]
Q_L	Liquid volumetric flow rate [m^3/s]
Q_{lf}	Volumetric liquid flux [$m^3/(m^2\ s)$]
R	Gas constant [J/(mol K)]
T	Temperature [K]
v_G	Interstitial gas velocity [m/s]
v_L	Interstitial liquid velocity [m/s]
x	Liquid phase molar fraction [-]
y	Gas phase molar fraction [-]
Z	Column Height [m]
z	Spatial coordinate [m]

Greek letters

γ	Column porosity [-]
ε	Enhancement factor [-]
ε_{inf}	Infinite enhancement factor [-]
ζ_G	Gas volume fraction (gas hold-up) [-]
ζ_L	Liquid volume fraction (liquid hold-up) [-]
η	Column capture efficiency [-]
μ_L	Liquid phase viscosity [Pa s]
μ_0	Water viscosity at the temperature of 20 °C = 0.0010 [Pa s]
μ_{H2O}	Water viscosity [Pa s]
μ_G	Gas phase viscosity [Pa s]
ν_{NH3}	NH_3 stoichiometric coefficient in R. 3 [-]
ϱ_G	Gas molar density [mol/m^3]
ϱ_L	Liquid molar density [mol/m^3]
$\dot{\varrho}_G$	Gas mass density [kg/m^3]
$\dot{\varrho}_L$	Liquid mass density [kg/m^3]
σ	Liquid phase surface tension [kg/s^2]
σ_{ct}	Critical surface tension of the packing material [kg/s^2]

Superscripts

in	Inlet conditions
eq	equilibrium conditions

Subscripts

G	referred to the gas phase
i	referred to the i^{th} species
j	referred to the j^{th} reaction
L	referred to the liquid phase
$\|_{z\ =\ z^*}$	Calculated at the coordinate z*

such as high regeneration energy demand, solvent degradation and equipment corrosion (Chehrazi and Moghadas, 2022). Precisely, contaminants typically present in flue gases along with CO_2, such as NO_X and SO_X, can form heat-resistant corrosive species like HCl and SO_2 as well as NO_2, that cause solvent degradation. For this reason, a pre-treatment process is usually required that, along with the high regeneration energy, invariably determines very high operational costs (Echevarria Huaman, 2015; Lawal et al., 2005; Zhao et al., 2012). Accordingly, several studies have been carried out in recent years to develop a cost-effective technology based on alternative solvents that can overcome these limitations. Many of these investigations identify aqueous ammonia solutions as one of the best CO_2 sorbents since they show higher CO_2 absorption capacity (Rivera-Tinoco and Bouallou, 2010) and significantly lower regeneration energy than amines. Moreover, NH_3 has the potential to react with several flue gas components (NO_x, SO_x and CO_2), once absorbed, so that specific byproducts, such as ammonium sulphate and ammonium nitrate that are commonly used as fertilizers (Powlson and Dawson, 2022), can be then recovered thus reducing the operating costs of the CO_2 capture process (Wang et al., 2017).

In the present work, the CO_2 absorption process via aqueous ammonia into a packed column is studied both experimentally and theoretically in order to develop a rate-based mathematical model capable to describe the capture process. The rate-based model consists of two different mass balances, one for the gas and one for the liquid phase, mathematically and physically interconnected by the mass transfer through the gas–liquid interface (Ramesh et al., 2007), rigorously modelled as suggested in the literature (Whitman, 1923). To quantitatively describe how the chemical reactions affect the liquid phase chemical composition, the approach proposed in our recent work (Atzori et al., 2023), that assumes that the relevant reactions taking place have reached the thermodynamic equilibrium, is integrated into the rate-based model. Such an aspect is usually not covered by most mathematical models for CO_2 absorption, with both aqueous ammonia (Chu et al., 2016; Li et al., 2014; Chu et al., 2017) and amine solutions (Saidi, 2017). In such works the solute consumption rate is typically assumed equal to the CO_2 transfer rate, thus without considering the occurring chemical transformations. Instead, the developed model describes how the liquid phase chemical composition changes during the process, allowing to evaluate the driving force variation for CO_2 and NH_3 mass transfer and thus accurately compute both the CO_2 absorption rate and the ammonia evaporation. By simulating the ammonia slip and by evaluating the sorbent solution chemical composition, the most important aspects of the entire separation process can be faced: sorbent regeneration and ammonia loss. Specifically, based on the chemical composition, the thermodynamic and physical features of the exhausted solution can be evaluated and used to properly select and design the best regeneration strategy. Above all, the model predictions can be used to minimize ammonia loss as much as possible by identifying the most appropriate operating conditions (e.g., system temperature).

The ordinary differential equation (ODE) system resulting from the proposed model of a counter-current process represents a two-boundary value problem whose solution is typically achieved by means of recursive algorithms that implement the shooting method, as also proposed in (Saidi, 2017; Afkhamipour and Mofarahi, 2013; Aboudheir et al., 2006), where the packed column system for the CO_2 absorption with different

amine solutions is addressed. To the best of our knowledge, a rate based mathematical model that quantitatively describes the packed column system for the CO_2 capture with ammonia aqueous solutions, along with the corresponding shooting method to solve the two-boundary value problem, is presented in this work for the first time. Finally, the proposed model is used as the key component for developing a model-aided algorithm for the packed column design. Based on the selected operating conditions, the algorithm relies on model results to perform an iterative calculation to determine the column height that allows to reach the capture specification (i.e., the capture efficiency).

2. Materials and methods

2.1. Materials

All reagents were used as received, without further purification. The diluted aqueous ammonia solutions were prepared from a concentrated aqueous ammonia solution (15.2 M, Sigma-Aldrich) and deionized water. Pure CO_2 (99.999 %) and N_2 (99.99 %) were provided by Rivoira Spa, and were mixed to simulate the composition of a flue gas (CO_2 10 $\%_{v/v}$). Flow rates of the gases were regulated by means of digital gas mass flow controllers (Aalborg) equipped with gas flowmeters (Cole Parmer). The CO_2 concentration in the gas mixture entering and exiting from the absorber was measured with a Varian CP-4900 gas chromatograph, equipped with a PoraPLOT U column (Agilent) and a thermal conductivity detector (TCD), and calibrated with 15 $\%_{v/v}$ and 40 $\%_{v/v}$ CO_2/N_2 reference mixture and 100 $\%_{v/v}$ CO_2 reference gas (Rivoira Spa).

2.2. CO_2 capture experiment

The CO_2 capture experiments were carried out by means of the apparatus depicted in Fig. 1. The absorber was a glass column (height 520 mm, internal diameter 40 mm) equipped with an external jacked and packed with glass rings (average dimensions: height 6 mm, internal diameter 4.5 mm, external diameter 6 mm, nominal size: 6 mm), for a total packing height of 400 mm. A thermostated liquid, circulating through the jacket of the column by means of a thermostatic bath (Julabo F33-MC, accuracy ± 0.1 °C), ensured that the desired temperatures (0–10 °C) were kept constant for the whole experiment. In this study, three experimental trials were conducted under different operating conditions and were repeated twice for the sake of reproducibility. Each experimental trial was divided into 10 consecutive steps, where the inlet NH_3 solution consisted of the outlet solution from the previous step. The experimental procedure is reported in Fig. 1, while the operating conditions for the different trials are shown in Table 1.

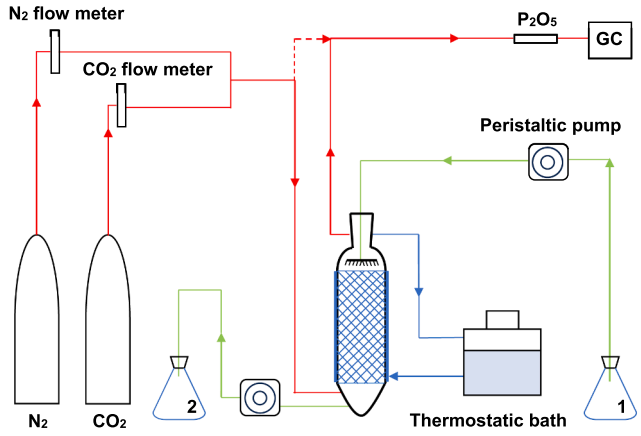

Fig. 1. Scheme of the process of carbon capture with aqueous ammonia solution.

Table 1
Operating conditions.

Exp	T [°C]	C^{in}_{NH3} [M]	Q_G [m^3/h]	Q_L [m^3/h]
1	10	1	$25.47 \bullet 10^{-3}$	$1.67 \bullet 10^{-3}$
2	0	1	$25.47 \bullet 10^{-3}$	$1.67 \bullet 10^{-3}$
3	0	2	$25.47 \bullet 10^{-3}$	$1.67 \bullet 10^{-3}$

In the first step of each experiment, 400 mL of fresh ammonia solution was prepared and stored in flask 1. At the start of the step, the absorber was fed from the top with the ammonia solution from flask 1 at the desired flow rate, regulated via a peristaltic pump (Masterflex). Countercurrent to the NH_3 solution flow, the gaseous CO_2/N_2 mixture was fed from the bottom of the column at a constant flow rate of 25.47 L/h (CO_2 = 10 $\%_{v/v}$; 0.00176 mol_{CO2}/min). After passing through the entire column, the CO_2-rich ammonia solution left the bottom of the column and was stored in flask 2 (Fig. 1). The vent gas leaving the top of the absorber was dried with a tower filled with P_2O_5 before being GC analyzed to determine the amount of CO_2 present in real time. By comparing the percentage of CO_2 in the gas mixture before and after the absorption, the capture efficiency was calculated. The step lasted as long as it took the transfer of the entire solution from flask 1 to flask 2. At the end of the first step, the second step begins, in which the column was fed with the solution now contained in flask 2. The same procedure was adopted for each subsequent step, where the absorbent solution was that one recovered from the previous step, for a total of 10 steps. The average absorption efficiency and the total amount (mol) of captured CO_2 were measured for each operating step.

2.3. Packing specific surface area

An essential parameter for the absorption rate modeling that strictly depends on packing type is the packing specific surface area (a) that, in this work, was experimentally evaluated for the glass rings. The specific surface area is defined as the ratio between the surface area of the single packing particle column volume it occupies. The surface area is easily calculated as the surface of the hollow cylinder, while the volume occupied by particles has been measured. After the vessel was randomly packed with the particles, by knowing both the number of particles needed to fill up the vessel (about 1950) and the vessel volume, the volume occupied by a single particle and also the number of particles in 1 m^3 could be calculated. From the values of the surface area of a single packing particle and the number of particles in 1 m^3, one could calculate the packing specific surface area. The obtained value (a = 704 m^2/m^3) was in accordance with the data of the specific area of Raschig rings dimensionally similar to glass rings used in this work (Perry et al., 1999).

3. Mathematical model

3.1. Mass transfer rate

To evaluate the mass transfer through the gas/liquid interface, according to the two-film theory, Eq. (1) is used:

$$J_i = K_{i,G}\left(p_i - p_i^*\right) \tag{1}$$

where J_i represents the molar flux (flow per unit surface), $K_{i,G}$ the gas overall mass transfer coefficient, p_i the partial pressure into the gas phase and p_i^* the equilibrium partial pressure, given by Eq. (2) (Rosenberg and Peticolas, 2004):

$$p_i^* = H_i \cdot C_i. \tag{2}$$

where H_i represents Henry constant of i^{th} *species* and C_i is the corresponding concentration into the liquid phase. Based on the two-film theory, both liquid and gas phase resistance need to be considered when evaluating mass transfer. Accordingly, $K_{i,G}$ should depend on the

Table 2
Chemical reactions into liquid phase.

Reaction	ID
$CO_2 + H_2O \Leftrightarrow^{K_1} HCO_3^- + H^+$	R.1
$HCO_3^- \Leftrightarrow^{K_2} CO_3^{2-} + H^+$	R.2
$2NH_3 + CO_2 \Leftrightarrow^{K_3} NH_2CO_2^- + NH_4^+$	R.3
$NH_3 + HCO_3^- \Leftrightarrow^{K_4} NH_2CO_2^- + H_2O$	R.4
$NH_3 + H_2O \Leftrightarrow^{K_{am}} NH_4^+ + OH^-$	R.5
$H_2O \Leftrightarrow^{K_w} OH^- + H^+.$	R.6

two local mass transfer coefficients of gas and liquid phase, $k_{i,G}$ and $k_{i,L}$, respectively, as shown in Eq. (3):

$$\frac{1}{K_{i,G}} = \frac{1}{k_{i,G}} + \frac{H_i}{\varepsilon k_{i,L}} \tag{3}$$

where ε is the enhancement factor needed to account for the reaction effects on the mass transfer rate.

3.2. Reaction mechanism

Once the carbon dioxide is absorbed by the liquid phase, it reacts with water and ammonia, following the reaction scheme reported in Table 2. Carbon dioxide dissolution determines pH reduction thus resulting in bicarbonate (HCO_3^-) and carbonate (CO_3^{2-}) ions formation (R.1, R.2), while carbamate ion (NH_2COO^-) is produced by reactions R.3 and R.4 that consume and transform most of the carbon transferred into the liquid phase, finalizing the chemical absorption.

The CO_2-NH_3 reaction system could potentially give rise to heterogeneous reactions involving solid chemicals. Nevertheless, due to the high water solubility of the species involved, such heterogeneous equilibria can be neglected. Accordingly, the reactive system is well described by the reactions shown in Table 2.

3.3. Enhancement factor

In order to incorporate the effects of chemical reactions on the CO_2 mass transfer, the enhancement factor (ε), defined as the ratio between the absorption rate in presence and in absence of chemical reactions, is considered (van Swaaij and Versteeg, 1992). Its rigorous determination would need the solution of the mass balances that take into account simultaneously mass transfer and chemical reactions into the liquid film and thus there is not a general analytical expression to calculate this value (Kierzkowska-Pawlak, 2012).

Alternatively, the enhancement factor can be calculated by means of approximated methods, that consider different absorption regimes, identified by taking into account the enhancement factor of an infinitely fast reaction (ε_{inf}) and the Hatta number (Ha). For a CO_2-NH_3 system, ε_{inf} can be evaluated through Eq. (4) (van Swaaij and Versteeg, 1992; Fang et al., 2015),

$$\varepsilon_{inf} = 1 + \left(\frac{D_{NH_3,L} C_{NH_3}}{\nu_{NH_3} D_{CO_2,L} \frac{p_{CO_2}}{H_{CO_2}}} \right) \tag{4}$$

where $D_{i,L}$ is the diffusion coefficient of the i^{th} species in the liquid phase and ν_{NH3} is the ammonia stoichiometric coefficient in the reaction involving CO_2 consumption (R. 3). The Hatta number, whose expression is reported in Eq. (5), represents the ratio between the maximum amount of consumed gas in the liquid film and the maximum amount of transferred gas in absence of reactions for the case when the bulk carbon dioxide concentration is zero (Kierzkowska-Pawlak, 2012):

$$Ha = \frac{\sqrt{k_{app} D_{CO_2,L}}}{k_{CO_2,L}} \tag{5}$$

where k_{app} is the apparent kinetic constant of the reactive phenomena that determine CO_2 consumption into the liquid phase, evaluated through the kinetic model proposed in (Qin et al., 2010).

Typically, in view of sorbent regeneration, the ammonia concentration never tends to zero. Accordingly, the absorption regime that occurs is the so-called *fast pseudo first order regime* that holds when $2 < Ha \ll \varepsilon_{inf}$ and allows to approximate the Enhancement factor as shown in Eq. (6) (Kierzkowska-Pawlak, 2012).

$$\varepsilon = \frac{Ha}{\tanh(Ha)} \tag{6}$$

It is well-known that the latter one tends to Ha if $Ha > 3$.

3.4. Model equations

Assumption

The multiphase system related to the CO_2 absorption by aqueous NH_3 into a packed column is described by means of the pseudo-single-liquid model, where the liquid phase is supposed to be pseudo-continuous. The model equations are based on the following assumptions:

1. Liquid phase is incompressible and the variation of both pressure and concentration range do not have a significant influence on liquid density which is then considered to be constant.
2. The boundary effects at the vessel walls can be neglected and liquid and gas phases properties are assumed to be uniform along the radial direction.
3. There is no axial o radial dispersion in the gas and liquid phase and the volumetric flow rates remain constant.
4. Liquid and gas interstitial velocity are assumed to be zero along the radial direction.
5. The capture column is operated under steady-state conditions.
6. The process of gas absorption is isothermal.
7. Liquid and gas velocity field are assumed to be uniform along the column.
8. Liquid phase is considered an ideal solution.

In order to develop the model equations governing the capture process along the column, the classical scheme, shown in Fig. 2, has been adopted.

In Fig. 2 the direction of the spatial domain, chosen to perform the calculation, is shown. It goes from the bottom (z = 0), to the top of the column (z = Z), with G and L representing the molar flow rate of gas and liquid, respectively.

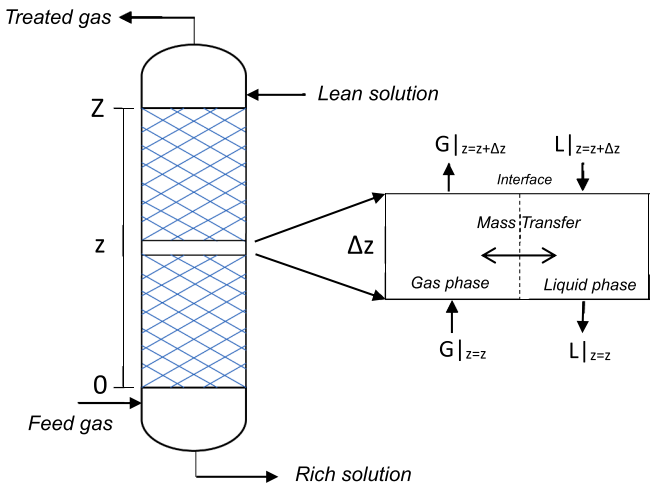

Fig. 2. Schematic representation of capture column and control volume.

Gas phase.

Based on the scheme presented in Fig. 2, the continuity equation for the gas phase can be written as reported in Eq. (7):

$$0 = \frac{d(v_G \zeta_G \varrho_G)}{dz} + \sum_{i=CO_2,NH_3} a_w K_{i,G}(p_i - H_i \bullet C_i) \tag{7}$$

where v_G is the interstitial gas velocity, ζ_G is the gas volume fraction (gas hold-up) and ϱ_G is the gas phase molar density. The second term in the right-hand side of Eq. (7) accounts for the molar transfer of carbon dioxide and ammonia through the gas/liquid interface. The molar flux is expressed with Eq. (1) and a_w represents the wetted surface area, defined as the transfer surface per unit volume of the column.

Moreover, to describe how the gas phase partial pressure of the i^{th} component changes, the molar balance for the single i species can be written as reported with Eq. (8):

$$0 = \frac{1}{RT}\frac{d(v_G \zeta_G p_i)}{dz} + a_w K_{i,G}(p_i - H_i \cdot C_i) \tag{8}$$

being T the absolute temperature and R the gas constant.

Liquid phase.

Based on the assumption (7), related to the liquid velocity field, and assumption (1), accounting for the constant liquid density, the liquid phase continuity equation can be approximated as follows:

$$0 = \frac{d(v_L \zeta_L \varrho_L)}{dz} \tag{9}$$

where ρ_L is the liquid phase density, v_L is the interstitial liquid velocity and ζ_L is the liquid phase volume fraction (liquid hold up) that can be related to ζ_G through the packing porosity, γ, by Eq. (10):

$$\gamma = \zeta_G + \zeta_L \tag{10}$$

Following the approach used in (Atzori et al., 2023; Concas et al., 2012, 2021) total carbon (C_t) concentration and total nitrogen (N_t) concentration in the liquid phase can be defined with Eq. (11) and Eq. (12), respectively:

$$C_{Ct} = C_{CO_2} + C_{HCO_3^-} + C_{CO_3^{2-}} + C_{NH_2CO_2^-} \tag{11}$$

$$C_{Nt} = C_{NH_3} + C_{NH_4^+} + C_{NH_2CO_2^-} \tag{12}$$

As proposed in (Atzori et al., 2023), since NH_3 and CO_2 are the only nitrogen-containing and carbon-containing species that cross the gas/liquid interface, the molar balances of total carbon, C_t, and total nitrogen, N_t, can be written as reported in Eq. (13) and Eq. (14), respectively:

$$0 = \frac{d(C_{C_t})}{dz} + \frac{a_w K_{CO_2,G}}{v_L \zeta_L}\left(p_{CO_2} - H_{CO_2} C_{CO_2}\right) \tag{13}$$

$$0 = \frac{d(C_{N_t})}{dz} + \frac{a_w K_{NH_3,G}}{v_L \zeta_L}\left(p_{NH_3} - H_{NH_3} C_{NH_3}\right) \tag{14}$$

Moreover, the electroneutrality equation, Eq. (15), is used to account for the solution neutrality and relate the ions concentrations into the solution:

$$0 = C_{H^+} - C_{OH^-} - C_{HCO_3^-} - 2C_{CO_3^{2-}} - C_{NH_2CO_2^-} + C_{NH_4^+} \tag{15}$$

Even though the rigorous description of the reactive phenomenon would need to take into account all reaction rate (direct and inverse) of (R.1-R.6), the fast dynamics of the reactive process, with respect to the mass transfer one, allows to assume that the reactions immediately achieve equilibrium conditions (Atzori et al., 2023). Accordingly, Eq. (11), Eq. (12) and Eq. (15) can be expressed as a function of C_{CO2}, C_{NH3} and C_{H+} by substituting the equilibrium relations (reported in the supplementary materials) and then obtain the equation system Eqs. (16)–(18). Note that the equilibrium constants (K_j with j [1, 2, 3, 4, w, am] and C_{H2O} keeps constant along the column height since the capture column is isothermal.

$$C_{C_t} = C_{CO_2} + \frac{K_1 C_{CO_2}}{C_{H^+}} + \frac{K_1 K_2 C_{CO_2}}{C_{H^+}^{\ 2}} + \frac{K_3 K_w C_{CO_2} C_{NH_3}}{C_{H^+} C_{H2O} K_{am}} \tag{16}$$

$$C_{N_t} = C_{NH_3} + \frac{K_{am} C_{NH_3} C_{H2O} C_{H^+}}{K_w} + \frac{K_3 K_w C_{CO_2} C_{NH_3}}{C_{H^+} C_{H2O} K_{am}} \tag{17}$$

$$0 = C_{H^+} - \frac{K_w}{C_{H^+}} - \frac{K_1 C_{CO_2}}{C_{H^+}} - 2\frac{K_1 K_2 C_{CO_2}}{C_{H^+}^{\ 2}} - \frac{K_3 K_w C_{CO_2} C_{NH_3}}{C_{H^+} C_{H2O} K_{am}} + \frac{K_{am} C_{NH_3} C_{H2O} C_{H^+}}{K_w} \tag{18}$$

As proposed by (Atzori et al., 2023), Eqs. (16)–(18) are derived with respect to the independent variable (spatial coordinate, z) to obtain an algebraic equation system, shown with Eqs. (19)–(21), whose unknowns are [dC_{CO2}/dz, dC_{NH3}/dz, dC_{H+}/dz]. The explicit derivation of Eqs. (19)–(21) is reported in the supplementary materials.

$$\frac{dC_{C_t}}{dz} = a_1\left(C_{CO_2}, C_{NH_3}, C_{H^+}\right)\frac{dC_{CO_2}}{dz} + b_1\left(C_{CO_2}, C_{NH_3}, C_{H^+}\right)\frac{dC_{NH_3}}{dz} + c_1\left(C_{CO_2}, C_{NH_3}, C_{H^+}\right)\frac{dC_{H^+}}{dz} \tag{19}$$

$$\frac{dC_{N_t}}{dz} = a_2\left(C_{CO_2}, C_{NH_3}, C_{H^+}\right)\frac{dC_{CO_2}}{dz} + b_2\left(C_{CO_2}, C_{NH_3}, C_{H^+}\right)\frac{dC_{NH_3}}{dz} + c_2\left(C_{CO_2}, C_{NH_3}, C_{H^+}\right)\frac{dC_{H^+}}{dz} \tag{20}$$

$$0 = a_3\left(C_{CO_2}, C_{NH_3}, C_{H^+}\right)\frac{dC_{CO_2}}{dz} + b_3\left(C_{CO_2}, C_{NH_3}, C_{H^+}\right)\frac{dC_{NH_3}}{dz} + c_3\left(C_{CO_2}, C_{NH_3}, C_{H^+}\right)\frac{dC_{H^+}}{dz} \tag{21}$$

For the sake of simplicity, the coefficients involved in Eqs. (19)–(21), that represent the partial derivatives of Eqs. (16)–(18) with respect to C_{CO2}, C_{NH3} and C_{H+}, are named as $\mathbf{a} = [a_1, a_2, a_3]$, $\mathbf{b} = [b_1, b_2, b_3]$, and $\mathbf{c} = [c_1, c_2, c_3]$. Accordingly, such coefficients depend on the instantaneous values of C_{CO2}, C_{NH3} and C_{H+} and their mathematical expression is given in full in the supplementary materials. The equation system Eqs. (19)–(21) is now solved to obtain Eqs. (22)–(24): the ordinary differential equations (ODEs) that describe the spatial profile of C_{CO2}, C_{NH3} and C_{H+}. In this work, the vector $\mathbf{f} = [f_1, f_2, f_3]$ is used to symbolize the right-hand side of Eqs. (22)–(24), whose explicit expression is reported in the Supplementary materials. It is worth noting that the constant terms of Eq. (19), dC_{Ct}/dz, and Eq. (20), dC_{Nt}/dz, given by Eq. (12) and Eq. (13), respectively, depend on p_{CO2} and p_{NH3}. Accordingly, the solution of Eqs. (22)–(24) needs to account for the gas phase mass balances for carbon dioxide and ammonia, reported with Eq. (25) and Eq. (26), respectively:

$$\frac{dC_{CO_2}}{dz} = f_1\left(p_{CO_2}, p_{NH_3}, C_{CO_2}, C_{NH_3}, C_{H^+}\right) \quad C_{CO_2}|_{z=Z} = C_{CO_2}^{\ in} \tag{22}$$

$$\frac{dC_{NH_3}}{dz} = f_2(p_{CO_2}, p_{NH_3}, C_{CO_2}, C_{NH_3}, C_{H^+}) \quad C_{NH_3}|_{z=Z} = C_{NH_3}{}^{in} \tag{23}$$

$$\frac{dC_{H^+}}{dz} = f_3(p_{CO_2}, p_{NH_3}, C_{CO_2}, C_{NH_3}, C_{H^+}) \quad C_{H^+}|_{z=Z} = C_{H^+}{}^{in} \tag{24}$$

$$\frac{dp_{CO_2}}{dz} = -\frac{RT}{v_G \zeta_G} a_w K_{CO_2,G}\left(p_{CO_2} - H_{CO_2} \bullet C_{CO_2}\right) \quad p_{CO_2}|_{z=0} = p_{CO_2}{}^{in} \tag{25}$$

$$\frac{dp_{NH_3}}{dz} = -\frac{RT}{v_G \zeta_G} a_w K_{NH_3,G}\left(p_{NH_3} - H_{NH_3} \bullet C_{NH_3}\right) \quad p_{NH_3}|_{z=0} = p_{NH_3}{}^{in} \tag{26}$$

The state variables can be also indicated with the variable vector $\mathbf{y} = [C_{CO2}, C_{NH3}, C_{H+}, p_{CO2}, p_{NH3}]$. Typically, the inlet conditions of both gas and liquid stream are known. On the other hand, in a counter-current absorption process, they refer to different coordinate, since the flue gas is fed at the bottom (z = 0) while absorption liquid on the top (z = Z) of the column, as shown in Fig. 2. Accordingly, the ODE system with the corresponding boundary conditions, expressed with Eqs. (22)–(26), represents a two-point boundary value problem, whose numerical solution is obtained by means of the shooting method, as discussed in section 4.

3.5. Physical parameters

Fluid dynamic parameters.

The liquid hold-up, defined as the ratio between the liquid and the actual column volume, is usually determined through empirical correlations that depend on the fluid dynamical regime. In this work, the Eq. (27) is used since the liquid volume flux is lower than $Q_{lf} = 40\ m^3\ m^{-2} h^{-1}$ (Fu et al., 2020; Suess and Spiegel, 1992):

$$\zeta_L = \frac{0.0169}{100} a^{0.83} Q_{lf}{}^{0.37} \left(\frac{\mu_L}{\mu_0}\right)^{0.25} \tag{27}$$

with μ_L representing the liquid phase viscosity at the process temperature, obtained through Eq. (28) where x_{NH3} represents the ammonia molar fraction into the solution (Frank et al., 1996) and μ_0 is the water viscosity at the temperature of 20 °C (0.0010 Pa s), calculated with Eq. (33)

$$\mu_L = \left(0.67 + 0.78 x_{NH_3}\right) 10^{-6} \exp\left(\frac{17900}{RT}\right) \tag{28}$$

According to the literature (Onda et al., 1968) (Wang et al., 2005), the Eq. (29) can be used to relate the wetted surface area, a_w, to the specific surface area, a,

$$a_w = a\left[1 - exp\left(1.45\left(\frac{\sigma_{ct}}{\sigma}\right)^{0.75}\left(\frac{L_g}{a\mu_L}\right)^{0.1}\left(\frac{L_g{}^2 a}{\dot{\varrho}_L^2 g}\right)^{-0.05}\left(\frac{L_g{}^2}{\dot{\varrho}_L a\sigma}\right)^{0.2}\right)\right] \tag{29}$$

where L_g represents the liquid mass flux, σ is the surface tension of the solution, σ_{ct} is the critical surface tension of the packing material, $\dot{\varrho}_L$ is the mass density of the liquid phase and g is the gravity acceleration.

Thermodynamic parameters.

The equilibrium constants of reactions R.1-R.6 are summarized in Table 3 (Atzori et al., 2023), while the equation used to calculate water concentration (C_{H2O}) is reported in the supplementary materials

The Henry constants accounting for the interface equilibrium both for carbon dioxide and ammonia are given by Eq. (30) and Eq. (31) (Sander, 2015), respectively:

$$H_{CO_2} = \left(53.3 + 0.00281 C_{NH_3}\right) exp\left[\frac{-1.206 \cdot 10^3}{T} + \frac{2350}{298.15}\right] \tag{30}$$

$$H_{NH_3} = \frac{1}{0.59} exp\left[-4200 \cdot \left(\frac{1}{T} - \frac{1}{298.15}\right)\right] \tag{31}$$

It is worth noticing that Eq. (30), accounting for the ammonia concentration effect on H_{CO2}, is obtained by considering the "N_2O analogy", proposed in the literature (Versteeg and Van-Swaaij, 1988), in addition to the relations inferred from (Qin et al., 2010; Sander, 2015; Seo et al., 2011).

The CO_2 diffusion coefficient in aqueous ammonia, $D_{CO2,L}$, was estimated by applying the modified Stokes–Einstein equation, where μ_{H2O} is the pure water solution viscosity and $D_{CO2,H2O}$ represents the CO_2 diffusion coefficient in pure water (Qin et al., 2010).

$$D_{CO_2,L} = D_{CO_2,H_2O}\left[\frac{\mu_{H_2O}}{\mu_L}\right]^{0.8} \tag{32}$$

$$\mu_{H_2O} = 1.18 \cdot 10^{-6} exp\left(\frac{16400}{RT}\right) \tag{33}$$

$$D_{CO_2,H_2O} = 2.35 \cdot 10^{-6} exp\left(\frac{-2119}{T}\right) \tag{34}$$

Finally, NH_3 diffusion coefficient is given by Eq. (35) (Poling et al., 2001):

$$D_{NH_3,L} = \frac{T \cdot 7.4 \cdot 10^{-8} \sqrt{2.6 MW_{H_2O}}}{\mu_{H_2O} \cdot 10^7 \cdot 24.96^{0.6}} \tag{35}$$

where MW_{H2O} represents the water molar weight.

Mass transfer coefficient.

Local liquid and gas phase mass transfer coefficient, as reported in

Table 3
Equilibrium constants.

Symbol	M.U.	$K_{eq}(T_{[K]})$	Reference
K_1	$\left[\text{mol m}^{-3}\right]$	$10^{\left(-\frac{3404.71}{T} + 17.8435 - 0.032786T\right)}$	(Perrin, 1969)
K_2	$\left[\text{mol m}^{-3}\right]$	$10^{\left(-\frac{2909.1}{T} + 9.119 - 0.02272T\right)}$	(Perrin, 1969)
K_3	$\left[m^3\ \text{mol}^{-1}\right]$	$C_{H2O} \bullet 10^{\left(+3.981 \cdot \frac{10^7}{T^3} - \frac{223620}{T^2} - \frac{348.71}{T} + 8.66 - 0.049T + 0.65\ln(T)\right)}$	(Atzori et al., 2023)
K_4	$\left[m^3\ \text{mol}^{-1}\right]$	$10^{-3} \bullet e^{\left(\frac{2900}{T} - 8.6\right)}$	(Edwards et al., 1978)
K_{am}	[−]	$e^{\left(-\frac{3335.7}{T} - 1.257 - 0.037057T + 1.497\ln(T)\right)}$	(Li et al., 2015)
K_w	$\left[\text{mol}^2\ \text{m}^{-6}\right]$	$10^{\left(-3.981 \cdot \frac{10^7}{T^3} + \frac{223620}{T^2} - \frac{3245.2}{T} + 2.098\right)}$	(Marshall and Franck, 1983)

(Perry et al., 1999), can be calculated as follows

$$k_{i,L} = 0.0051\left(\frac{\dot{\varrho}_L}{\mu_L g}\right)^{-1/3}\left(\frac{L_g}{a_w \mu_L}\right)^{2/3}\left(\frac{\mu_L}{\dot{\varrho}_L D_{i,L}}\right)^{-1/2}(a d_p)^{0.4} \quad (36)$$

$$k_{i,G} = 5.23\left(\frac{aD_{i,G}}{RT}\right)\left(\frac{G_g}{a\mu_G}\right)^{0.7}\left(\frac{\mu_G}{\dot{\varrho}_G D_{i,G}}\right)^{1/3}(a d_p)^{-2} \quad (37)$$

where d_p is the nominal diameter of the packing particle, μ_G is the gas viscosity, $\dot{\varrho}_G$ is the mass density of the gas phase, $D_{i,G}$ is the diffusion coefficient of the i^{th} species into the gas phase and G_g is the gas mass flux.

4. Model solution

The design algorithm for the column height calculation consists in two nested loops, separately shown in Fig. 3 and Fig. 4, for the sake of simplicity.

Shooting method.

The external loop (Fig. 3) implements the shooting method, needed to manage the two-boundary value problem, and thus solve the model equations (22)–(26), whose results are used in the internal loop (Fig. 4) that actually performs the column height calculation. Specifically, the column capture efficiency (η), chosen as the design specification in the column height calculation, is defined in terms of CO_2 absorbed along the column (z ∈ [0, Z]), with respect to the corresponding inlet value, according to Eq. (38):

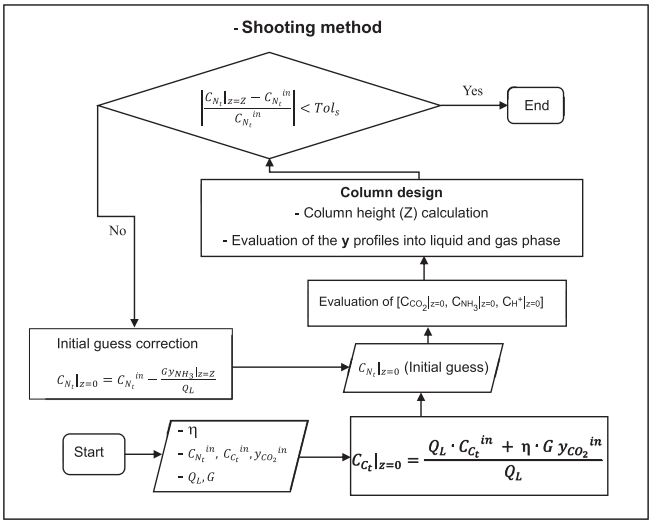

Fig. 3. The shooting method adopted.

$$\eta = \frac{Gy_{CO_2}^{in} - Gy_{CO_2}|_{z=Z}}{Gy_{CO_2}^{in}} \quad (38)$$

where y_{CO2}^{in} is the inlet molar fraction of CO_2 in the gas phase. i.e., at z = 0. The gas molar flow can be easily calculated as $G = ¼\, v_G\, \zeta_G\, \varrho_G\, \pi d_C^2$, where d_C is the internal column diameter and ϱ_G can be obtained through Eq. (7).

The shooting method, reported in Fig. 3, is used to transform the two-boundary value problem, expressed in Eqs. (22)–(26), into an initial value problem to be solved through a recursive algorithm. The integration is performed from z = 0 with p_{CO2}^{in} and p_{NH3}^{in} as boundary values of Eq. (25) and Eq. (26), respectively.

Based on the shooting method procedure, the boundary conditions at z = 0 of Eqs. (22)–(24) are initially guessed and successively corrected in order to meet the known boundary conditions at z = Z. The recursive procedure is described below.

Firstly, the capture efficiency value, η, selected as design specification, is used to evaluate the first value of the carbon concentration at z = 0, $C_{Ct}|_{z=0}$. In fact the latter one can be obtained under steady state conditions, through Eq. (39), since the inlet values C_{Ct}^{in} and y_{CO2}^{in} as well as the operating conditions Q_L and G are known,

$$C_{C_t}|_{z=0} = \frac{Q_L \cdot C_{C_t}^{in} + \eta \cdot G y_{CO_2}^{in}}{Q_L} \quad (39)$$

which clearly represents a macroscopic material balance on the total carbon within the liquid phase.

Once $C_{Ct}|_{z=0}$ is evaluated, the total nitrogen concentration at z = 0 ($C_{Nt}|_{z=0}$) is initially guessed and, together with $C_{Ct}|_{z=0}$, is substituted in the algebraic equation system, Eqs. (16)–(18), to determine the (guessed) boundary conditions [$C_{CO2}|_{z=0}$, $C_{NH3}|_{z=0}$, $C_{H+}|_{z=0}$] of Eqs. (22)–(24). It should be noted that the initial guess value of $C_{Nt}|_{z=0}$ is chosen to be equal to C_{Nt}^{in}.

The ODE system of Eqs. (22)–(26) can be then solved as an initial value problem by performing the relevant integration from z = 0 and its results are used to evaluate the column height, as described next (column design section). In the present work, it was solved through the subroutine ODE45 which takes advantage of the Runge-Kutta (4,5) method on Matlab.

Once the column height and the spatial profiles of the state variables (**y**) are obtained, since C_{NH3} and p_{NH3} profiles along the column height are known, Eq. (14) can be used to evaluate the actual value of $C_{Nt}|_{z=Z}$. If its relative difference with respect to C_{Nt}^{in} exceeds a defined tolerance ($Tol_s = 10^{-8}$ as reported in the decision block of the algorithm shown in Fig. 3), the guess value ($C_{Nt}|_{z=0}$) is corrected and the calculation is performed again. Specifically, the guess value correction is performed based on the macroscopic material balance on the total nitrogen, which can be written as reported in Eq. (40), since we are dealing with a steady-state process where the ammonia molar fraction in the inlet gas

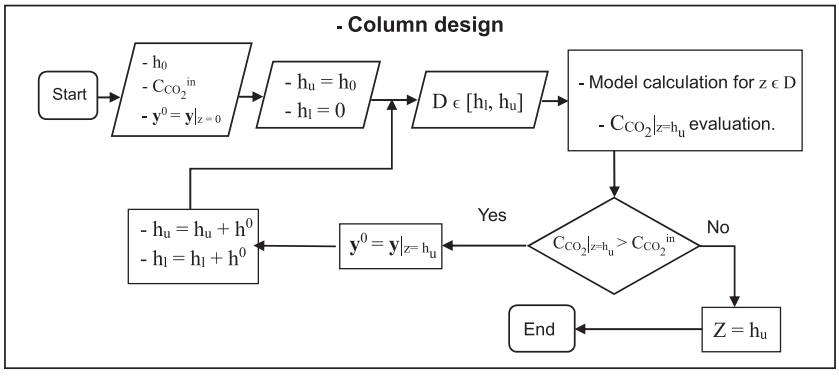

Fig. 4. Column height evaluation.

stream is zero ($y_{NH3}|_{z=0}$) and NH_3 is the only nitrogen-containing species in the gas phase.

$$Q_L \cdot \left(C_{N_t}|_{z=Z} - C_{N_t}|_{z=0}\right) = G \cdot y_{NH_3}|_{z=Z} \quad (40)$$

Eq. (40) shows that the difference in total nitrogen concentration between the top and column bottom is directly proportional to ammonia losses. Accordingly, the latter one, i.e. $G \cdot y_{NH3}|_{z=Z}$, is used to correct the guess value by taking into account the known value of the nitrogen concentration at the column top (C_{Nt}^{in}). As a result, by referring to Eq. (40), and considering the inlet value, $C_{N_t}|_{z=Z} = C_{Nt}^{in}$, that is known as an operating condition, and $y_{NH3}|_{z=Z}$, calculated by the model in the j^{th} iteration, the guess value for the next (j^{th+1}) iteration is corrected as $C_{Nt}|_{z=0} = C_{Nt}^{in} - (G \cdot y_{NH3}|_{z=Z})/ Q_L$.

Column design.

It is apparent that, once the initial conditions, $\mathbf{y}^0 = \mathbf{y}|_{z=0}$, are known, the model equations, Eqs. (22)–(26) can be numerically solved as an initial value problem and the spatial profiles of the state variables, $\mathbf{y}(z)$, can be evaluated within the defined spatial domain, D. Referring to Fig. 4, let h_0 be the spatial step size of the algorithm, used to define the first spatial domain, $D = [h_l, h_u]$, with h_l and h_u firstly equal to 0 and h_0, respectively. Once the model equations, Eqs. (22)–(26), are solved and thus the spatial profiles ($\mathbf{y}(z)$ with $z \in D$) are computed, it is possible to verify if $C_{CO2}|_{z=hu}$ results to be larger than the operating inlet condition, C_{CO2}^{in}. Then the spatial domain (D) is increased by the step size (h_0), while the final values of the state variables ($\mathbf{y}|_{z=hu}$) are used as the initial values for the successive integration. This procedure is iterated until the prescribed condition, i.e. $C_{CO2}|_{z=hu} \leq C_{CO2}^{in}$, is satisfied. Consequently, the calculated column height corresponds to the current upper boundary h_u of the spatial domain.

In order to verify the robustness of the result, the step size (h^0) is halved and the calculation is repeated until the relative variation of the calculated column height is lower than a certain tolerance: 10^{-8}.

It is apparent that the developed procedure actually consists of two nested loops, which in turn takes an additional external loop into account needed to allow the algorithm convergence. As demonstrated in the supplementary materials, the choice to propose such algorithm which takes advantage of consecutive column layers, allows to reduce the computational cost by a factor of (N + 1)/2 with respect to the method that performs the integration from z = 0 during each iteration, being $N = Z/h_0$ the number of column layers needed to fulfill the prescribed efficiency.

It is worth mentioning that implementing the shooting method from scratch is not the only way to solve a boundary value problem. Indeed, computing platforms such as Matlab provide bult-in functions for solving boundary value problems (bvp5c or bvp4c). The main reason why such built-in functions are not used in this work is the will to develop a resolution framework as reproducible as possible, irrespectively of the programming language or numeric computing software used to solve the problem. The implementation of a a simple iterative process such as the shooting method, allows to easily handle boundary value problems without pre-programmed functions. Indeed, albeit the latter may be more performable than the shooting method, they may not be available in specific computing platforms or may be embedded at a level such that the modulation of internal parameters or functions is not possible, as is the case with bvpc5c and bvp4c in Matlab. Accordingly, by programming the boundary value problem solution from scratch, one has complete control on the solution calculation, both because the tolerance parameter or the correction factor can be easily changed, but also because one is not constrained to rely on the solution method embedded in the solver being used.

5. Results

In order to evaluate the algorithm design performance and test the model accuracy, the experimental results of capture efficiency (η) have been used as input data for the design algorithm. As explained in section 2, each experimental trial is divided in 10 different steps during which the system temperature, the liquid and gas flow rate and the inlet gas composition are kept constant, whereas the capture efficiency and the inlet CO_2 loading (defined as the ratio between C_{Ct} and C_{Nt}) change step by step. Specifically, the outlet liquid stream that, at the end of the i^{th} capture step, is sent to the tank 2 and will be used as the inlet liquid stream in the next capture step, $(i + 1)^{th}$, has a different (higher) CO_2 loading with respect to the inlet liquid stream of the i^{th} capture step. As a consequence, the capture efficiency at the end of the i^{th} step will be different (higher) than the one of the $(i + 1)^{th}$ capture step. This procedure provides as many different experimental tests as the steps being carried out, for each experimental trial (Exp. 1, Exp. 2, Exp. 3). To summarize, during the single experiment trial, two operating conditions change step by step:

- the capture efficiency, experimentally measured for the specific step (η_i);
- the CO_2 loading of the inlet liquid stream, calculated based on the cumulative measurements of the absorbed CO_2 related to the capture steps preceding the step under consideration.

As reported in Table 1, three different experimental trials, consisting of 10 steps, have been performed. With this approach, 30 different efficiency measurements for 30 different experimental conditions have been obtained. Since any single experimental trail is repeated twice (trial A and trial B), for the sake of reproducibility, the experimental result related to the measured capture efficiency, reported in Table 4, consists of two columns (A and B) for each of them.

The efficiency values, reported in Table 4, along with the corresponding operating conditions, shown in Table 1, are used as inputs in the design algorithm to compute the packing height. The capture device where the CO_2 separation process is performed has a defined height (0.4 m) that, consequently, is the value the design algorithm should provide (dashed line in Figs. 5–7). In this section, the comparison between the height calculated by the algorithm and the capture device actual height are compared for each experimental test (Figs. 5–7). Each figure shows two series of calculated values (A and B), due to the two series of measured efficiency values (η) for each experiment.

The results reported in Figs. 5–7 demonstrate the performance of the design algorithm that manages to approximate the actual height of the capture device with good accuracy for the three experimental trials, in spite of the variation of operating conditions such as system temperature and ammonia inlet concentration. The comparison between model results and experimental data related to the third series of experimental trial is on the other hand less satisfactory respect to the previous ones due to the higher values of efficiency (Table 4), used as input to perform the height calculation. Indeed, the higher the efficiency achieved, the lower the outlet p_{CO2} in the gas phase and then the lower the driving force for the CO_2 transfer at the column top. Accordingly, as the efficiency increases, the absorption rate decreases at the column top and the

Table 4
Experimental results expressed in terms of evaluated efficiency.

Step	η_{Exp1} [%]		η_{Exp2} [%]		η_{Exp3} [%]	
	A	B	A	B	A	B
1	88.57	89.55	92.02	91.28	98.92	98.94
2	84.80	84.86	81.19	79.68	99.11	98.83
3	77.14	78.44	73.85	71.05	98.40	97.21
4	78.89	76.04	67.14	61.31	97.40	93.35
5	67.99	70.97	58.11	58.45	95.89	90.18
6	63.30	62.95	56.96	55.49	92.04	89.38
7	54.17	56.08	49.53	53.16	88.94	85.26
8	48.05	52.08	45.35	49.97	84.40	80.92
9	45.57	48.04	39.83	46.24	78.59	76.85
10	39.85	43.81	38.36	41.13	75.70	70.98

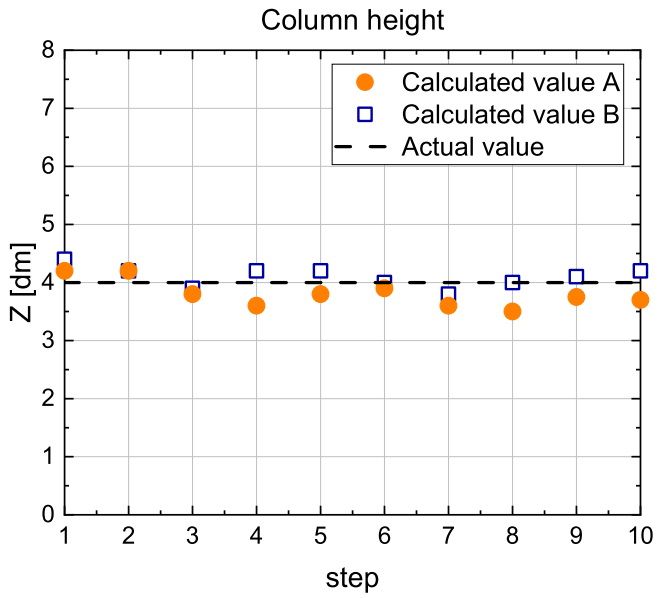

Fig. 5. Comparison between column actual height (0.4 m) and the one evaluated through the proposed design method at the end of each step of Experiment 1. MSE = 0. 064.

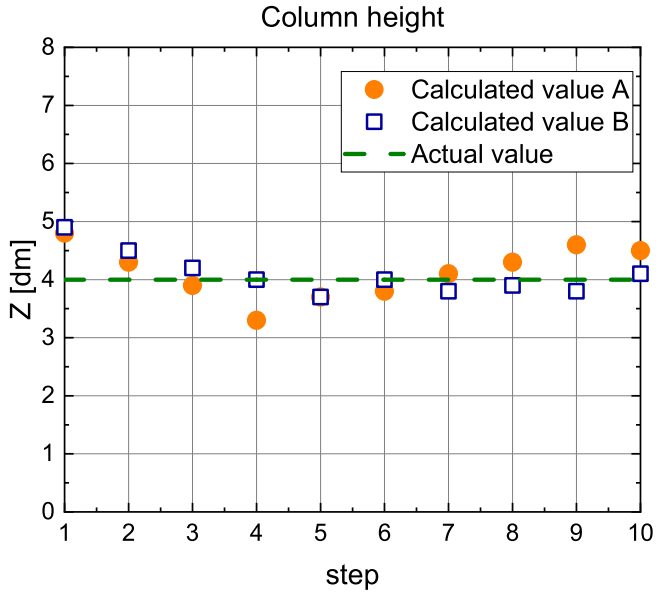

Fig. 6. Comparison between column actual height (0.4 m) and the ones evaluated through the proposed design method at the end of each step of Experiment 2. MSE = 0.176.

column height value calculation becomes highly sensitive to changes in efficiency. As a result, the measurement error in estimating the capture efficiency determines higher variation in the height calculated by the model.

However, the design algorithm output is not limited to the column height evaluation. With Eq. (22), C_{CO2} profile can be computed and CO_2 loading can be easily obtained through its definition (C_{Ct}/C_{Nt}). Moreover, once the spatial profiles of C_{CO2}, C_{NH3} and C_{H+} are obtained through Eqs. (22)–(24), the concentration profiles of the remaining species involved in the reactive process can be calculated by means of the equilibrium relations (reported into the supplementary materials). In this regard, the following Fig. 8 shows how the chemical composition of the sorbent solution and the carbon content into the simulated flue

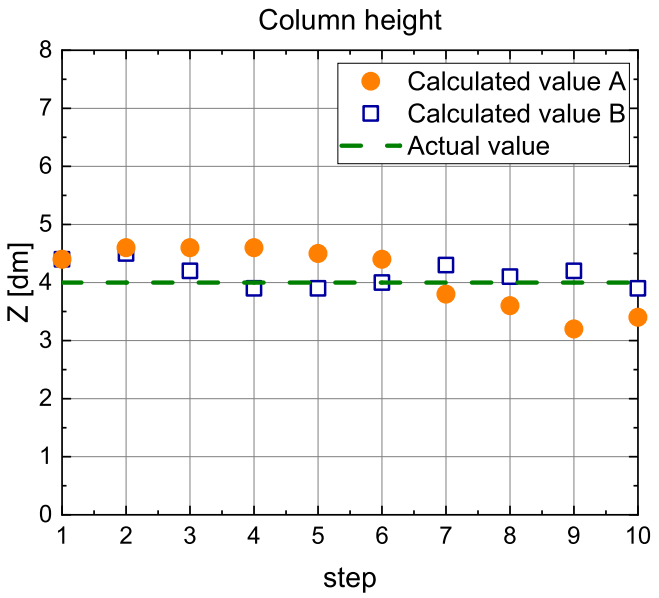

Fig. 7. Comparison between column actual height (0.4 m) and the ones evaluated through the proposed design method at the end of each step of Experiment 3. MSE = 0.224.

gas change both in the single step and during the entire Exp. 1. In Fig. 8a the liquid phase ion speciation is reported, including the three main ionic species (CO_3^{2-}, HCO_3^-, NH_2COO^-) while in Fig. 8b the CO_2 loading corresponding to the same experiment is shown. Due to the experimental strategy adopted, CO_2 step by step accumulates into the liquid phase, resulting in the increase of the CO_2 loading (Fig. 8b) and the continuous and gradual perturbation of the equilibria among the species (Fig. 8a).

At the beginning of the experimental trial, the strong alkalinity of the solution brings about the exclusive production of the carbonate ion (CO_3^{2-}) (Fig. 8c). Subsequently, as the CO_2 is absorbed, the liquid pH decreases (Fig. 8c) resulting in a shift of the R.2 equilibrium toward reagents which promotes the production of HCO_3^- and NH_2COO^-. Finally, the decrease of the absorption capacity between the different steps can be easily noticed in Fig. 8d. During the single step, y_{CO2} decreases due to CO_2 absorption, however, as the steps come in succession and the CO_2 loading increases, the capture capacity of the liquid diminishes, as shown in Fig. 8d, where the y_{CO2} variation in the single step is progressively smaller as the steps proceed.

The model analysis can also focus on the single step by describing how the chemical absorption process evolves along the column height.

Fig. 9a and b show the model prediction related to CO_2 loading and J_{CO2}, that represents the CO_2 molar flux at the interface.

As it can be seen, the C_{CO2} increase determines the CO_2 loading growth and the driving force reduction, that in turn results in J_{CO2} decrease. At the same time, the dissolved CO_2 is transformed by the liquid phase reactions that give rise to carbonic ion formation whose spatial profiles are reported in Fig. 9c. Finally, the ammonia evaporation reduces the total nitrogen content within the liquid phase increasing the ammonia molar fraction into the gas flow (y_{NH3}), as shown in Fig. 9d where the initial rapid growth of y_{NH3}, due to the high driving force, is followed by a slower increase when the equilibrium between gas and liquid phase (y_{NH3}^{eq}) is achieved.

These results can be useful in view of plant design. The knowledge of the chemical composition of the exhausted stream (Fig. 9) could be used to optimize the entire capture and regeneration processes by evaluating the thermodynamic properties of the stream and thus selecting the best regeneration strategy.

Finally, the model results can be used to identify the operating conditions range to minimize the NH_3 make-up stream thus reducing the

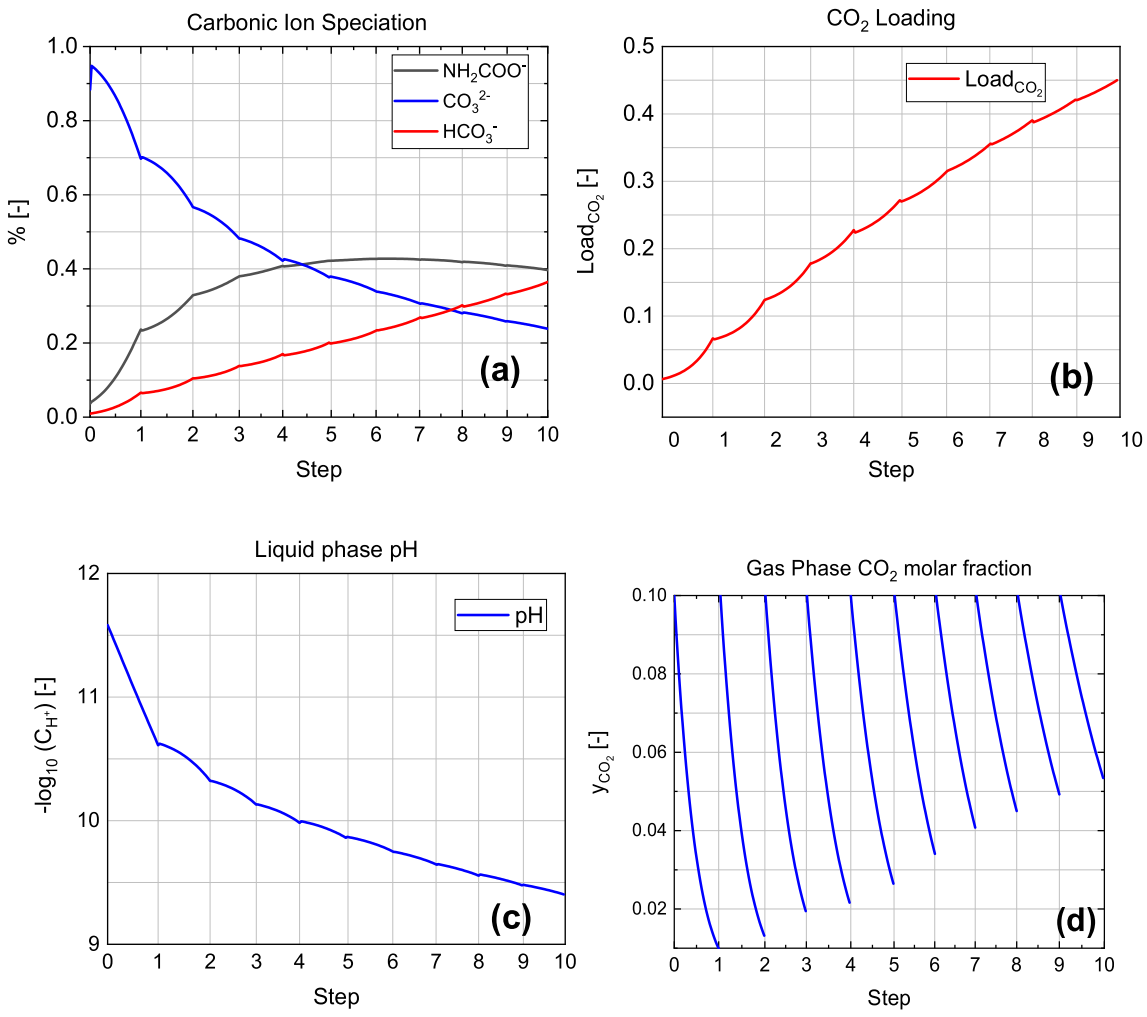

Fig. 8. Model predictions for Exp. 1. (a) Ion speciation in the liquid phase; (b) CO_2 Loading; (c) pH of the liquid; (d) CO_2 molar fraction in gas phase.

process costs. The temperature increase influences both the molecular diffusivity, resulting in larger mass transfer coefficients, and gas solubility in the liquid phase that decreases with the temperature. Nevertheless, as reported in (Zeng et al., 2013), in the temperature range 0–40 °C, the temperature effect on CO_2 mass transfer coefficient predominates on solubility reduction, showing an overall growth of the absorption rate that allows to reach the desired efficiency with lower column. However, the temperature increase also brings about the ammonia loss increment since it results in the simultaneous NH_3 solubility decrease and the NH_3 mass transfer growth. Accordingly, the operating temperature turns out to be a crucial parameter whose value has to be identify to optimize the process. In particular, Fig. 10 shows an example where the model is used to calculate both NH_3 loss (G^{out}_{NH3}) and column height (Z) as a function of absorption temperature. The capture efficiency is set at $\eta = 0.85$, the operating conditions such as gas and liquid flow rate, column diameter and packing type are the same as in the experimental trials discussed in section 2, while initial ammonia concentration is set equal to 1 M. The graph in Fig. 10 displays how the temperature increase allows to reduce the column height while, at the same time, increases the ammonia loss. Typically, the flue gas to be treated must be cooled down before the absorption, generating an energy demand that is as high as the absorption temperature is low. Nevertheless, as shown by Fig. 10, the lower the temperature, the lower the ammonia loss and thus the lower the costs in terms of NH_3 make up stream. With this in mind, the model prediction can help to identify the absorption temperature needed to minimize the overall costs, finding a trade-off value between the operating costs due to energy demand related to the flue gas cooling, the column manufacturing costs and the ammonia make-up stream operating costs.

According to the current literature, the most interesting approaches to model the packed columns for CO_2 chemical absorption with NH_3 are presented by authors (Chu et al., 2016; Li et al., 2014), who developed detailed fluid dynamic simulations based on the computational mass transfer model (CMT), solved with specific software as use the commercial software FLUENT. Another approach proposed in the literature (Niu et al., 2012; Qi et al., 2013) relies on the use the RateFrac module on ASPEN.

As far as the first approach is concerned, the model predictive capability is evaluated by comparing the experimental data of CO_2 mass fraction along the column height with model results, for three different sets of operating conditions (Li et al., 2014). The results show a good agreement between model prediction and experimental data, but no statistical parameter is presented to quantify the model accuracy. Moreover, the volumetric overall mass transfer coefficients are evaluated with an empiric relation whose parameters are fitted based on the specific experimental operating conditions such as CO_2 partial pressure, volumetric flow rate of aqueous ammonia solution, and aqueous ammonia concentration. Such an aspect limits the model applicability within the experimental range considered to identify the parameter. Moreover, as claimed by the authors (Li et al., 2014), to apply the proposed correlation to the industrial-scale structured packing, a scale-up factor involving packing geometry might be required. Moreover, the model capability evaluation is carried out using experimental results obtained in the same conditions used to fit the $K_G a_e$ correlation

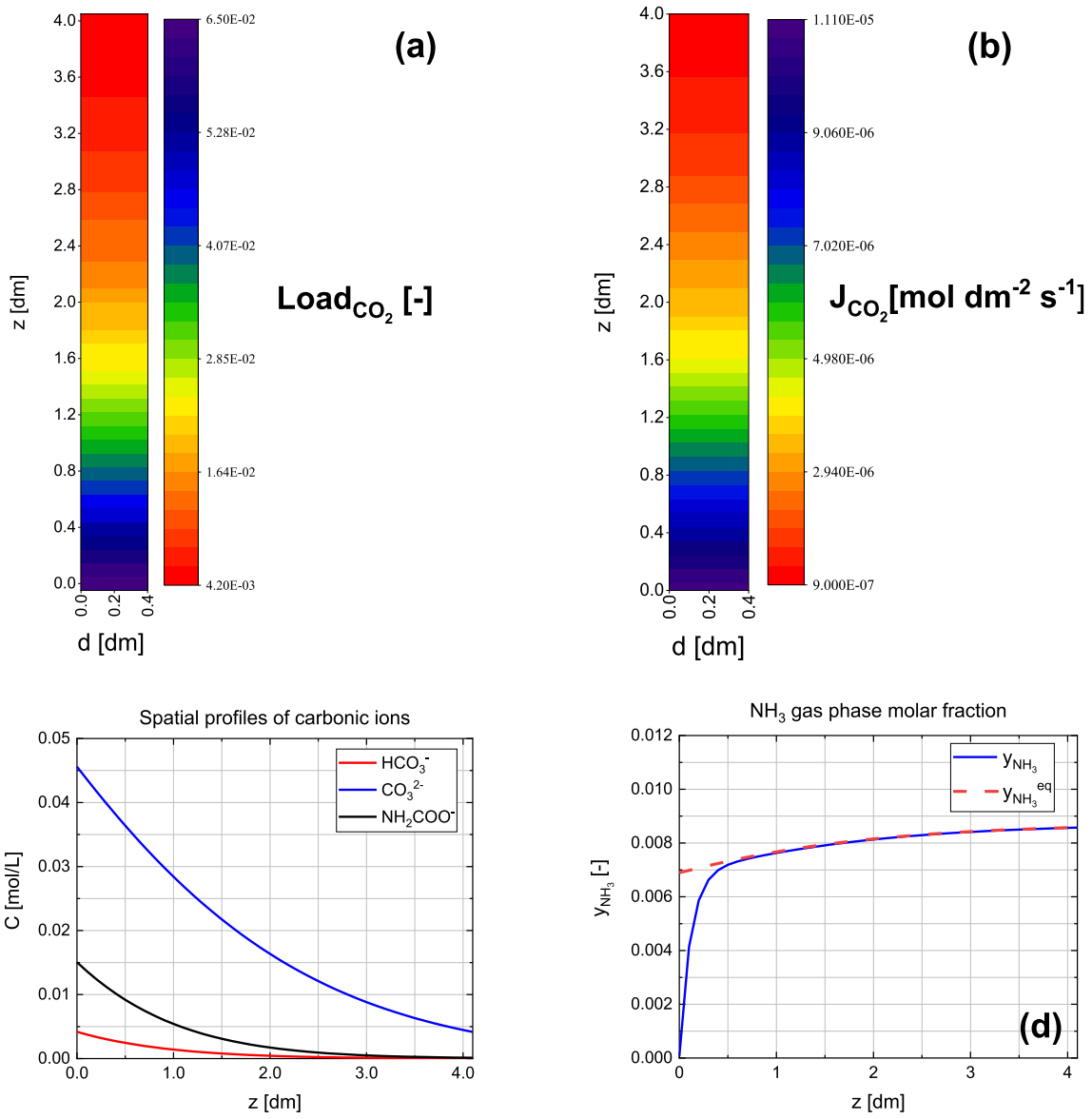

Fig. 9. Model prediction of the first step of Exp. 1. (a) CO_2 Loading; (b) CO_2 molar flux at the gas/liquid interface; (c) Liquid phase ion speciation; (d) Gas phase NH_3 molar fraction.

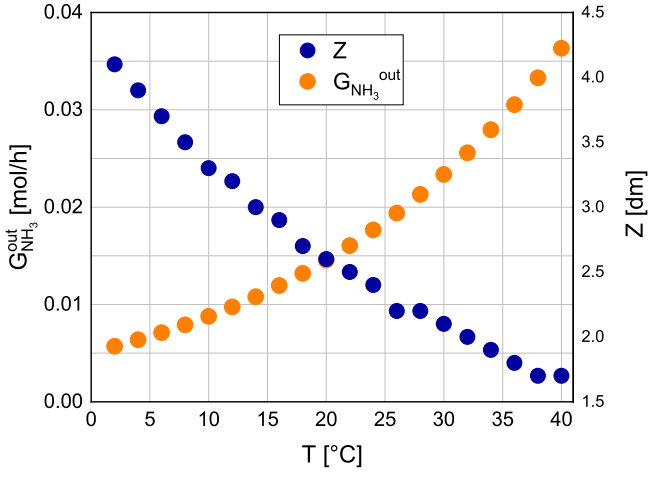

Fig. 10. Column height and ammonia loss with respect T.

parameter, hindering an actual validation of the model.

In the second approach, the absorption column is modeled with RateFrac, the rate-based distillation module of Aspen Plus (Niu et al., 2012; Qi et al., 2013). This approach requires a rigorous thermodynamic model, a rate model, and transport property models to be implemented in Aspen Plus. In both thermodynamic and rate model, the reaction mechanism (R1-R6) is taken into account to evaluate C_{CO2} and C_{NH3} and thus the driving force for CO_2 uptake and NH_3 evaporation, as the process evolves. As a consequence, this second approach turns out to be more similar to the model solution proposed in the present work. In particular, Qi et al., (2013) evaluate the absorption model effectiveness by comparing the experimental and model results in terms of CO_2 absorption rate, obtaining a quite satisfactory agreement, despite, even in this case, a quantitative evaluation of the model accuracy is not presented. Moreover, the absorption data used by Qi et al (2013) correspond to the average value along the absorbent column and they are not punctual value corresponding to a precise coordinate. Niu et al., (2012) simulated the variation of the capture efficiency along the column height obtaining a good agreement between experimental and simulated results, except for an offset at intermediate values of efficiency.

Specifically, in the first sections of the capture column, where CO_2 loading of sorbent solution is low, the simulated capture efficiency well captures the experimental data. However, as CO_2 loading gets larger, the mismatch increases, up to the last sections of the column, where the flue gas is nearly purified, and the efficiency approaches 100 %. In such sections the offset decreases and the correspondence between prediction and experimental data improves. Such an offset is probably due to an inconsistency between the actual reaction mechanism and rection model taken into account in the rate model for the $NH_3 - CO_2 - H_2O$ system. Even in this case, the graphical results are not supported by any parameter that allows to determine the model accuracy.

6. Conclusions

In this work, the CO_2 chemical absorption with aqueous ammonia in a packed column system has been experimentally investigated in order to develop a novel mathematical model useful to describe the CO_2 separation process from flue gas along the capture device. Such a model is then exploited to implement an algorithm for the column design (column height calculation) that has been validated by considering different combinations of operating conditions and capture efficiency specification. In particular, a capture column with a packing height of 40 cm was used to perform consecutive experimental tests to collect data on capture efficiency of the column for different combination of system temperature, initial ammonia concentration and CO_2 loading. The experimental values of the efficiency were then used as design algorithm input to calculate the column height. The calculated heights, obtained as algorithm output, were very close to the actual column height thus confirming the effectiveness and the reliability of the developed tool that managed to accurately estimate the packing height for several value of efficiency end different combination of operating conditions. Furthermore, the developed model allows to integrally describe the absorption process, evaluating also the ammonia slip and the chemical composition of the exhausted solution that turn out to be critical factors in view of ammonia recovery and sorbent regeneration. The rate-based model, coupled with the thermodynamical analysis of the liquid phase equilibria, proposed in this work, allows to precisely quantify the chemical composition of the sorbent solution and thus to evaluate the driving force for the CO_2 absorption and ammonia slip. In view of design an industrial plant, that should include a regeneration section, an ammonia make-up stream and flue gas colling process, such a calculation could be used to evaluate the exhausted solution physical properties to determine the most suitable regeneration strategy or identify the operating temperature that minimize the operating cost related to the sum of ammonia make-up and energy demand of the cooling process.

CRediT authorship contribution statement

Federico Atzori: Conceptualization, Data curation, Investigation, Methodology, Software, Validation, Writing – original draft, Writing – review & editing. **Francesco Barzagli:** Conceptualization, Investigation, Methodology, Resources, Writing – review & editing. **Suzhou Dai:** Data curation, Investigation, Resources, Writing – review & editing. **Alessandro Concas:** Conceptualization, Methodology, Supervision, Validation, Writing – original draft, Writing – review & editing. **Giacomo Cao:** Resources, Validation, Writing – review & editing.

Declaration of competing interest

The authors declare that they have no known competing financial interests or personal relationships that could have appeared to influence the work reported in this paper.

Data availability

Data will be made available on request.

Acknowledgements

One of us (G.C.) recalls with fond memory his activities as PhD student under the direction of professor Massimo Morbidelli. F.A. was supported by an International PhD Program in Innovation Sciences and Technologies at the University of Cagliari, Italy.

Appendix A. Supplementary data

Supplementary data to this article can be found online at https://doi.org/10.1016/j.ces.2024.119780.

References

Aboudheir, A., Tontiwachwuthikul, P., Idem, R., 2006. Rigorous model for predicting the behavior of CO2 absorption into AMP in packed-bed absorption columns, in: Industrial and Engineering Chemistry Research. https://doi.org/10.1021/ie050570d.

Afkhamipour, M., Mofarahi, M., 2013. Comparison of rate-based and equilibrium-stage models of a packed column for post-combustion CO2 capture using 2-amino-2-methyl-1-propanol (AMP) solution. Int. J. Greenh. Gas Control. https://doi.org/10.1016/j.ijggc.2013.02.022.

Atzori, F., Barzagli, F., Varone, A., Cao, G., Concas, A., 2023. CO2 absorption in aqueous NH3 solutions: Novel dynamic modeling of experimental outcomes. Chem. Eng. J. https://doi.org/10.1016/j.cej.2022.138999.

Chehrazi, M., Moghadas, B.K., 2022. A review on CO2capture with chilled ammonia and CO2utilization in urea plant. J. CO2 Util. https://doi.org/10.1016/j.jcou.2022.102030.

Chu, F., Jon, C., Yang, L., Du, X., Yang, Y., 2016. CO 2 Absorption Characteristics in ammonia solution inside the structured packed column. Ind. Eng. Chem. Res. https://doi.org/10.1021/acs.iecr.5b03614.

Chu, F., Liu, Y., Yang, L., Du, X., Yang, Y., 2017. Ammonia escape mass transfer and heat transfer characteristics of CO2 absorption in packed absorbing column. Appl. Energy. https://doi.org/10.1016/j.apenergy.2017.08.167.

Concas, A., Lutzu, G.A., Pisu, M., Cao, G., 2012. Experimental analysis and novel modeling of semi-batch photobioreactors operated with Chlorella vulgaris and fed with 100%(v/v) CO 2. Chem. Eng. J. 213, 203–213. https://doi.org/10.1016/j.cej.2012.09.119.

Concas, A., Lutzu, G.A., Turgut Dunford, N., 2021. Experiments and modeling of komvophoron sp. growth in hydraulic fracturing wastewater. Chem. Eng. J. https://doi.org/10.1016/j.cej.2021.131299.

Crippa, M., Guizzardi, D., Banja, M., Solazzo, E., Muntean, M., Schaaf, E., Pagani, F., Monforti-Ferrario, F., Olivier, J., Quadrelli, R., Risquez Martin, A., Taghavi-Moharamli, P., Grassi, G., Rossi, S., Jacome Felix Oom, D., Branco, A., San-Miguel-Ayanz, E., 2022. CO2 emissions of all world countries.

Echevarria Huaman, R.N., 2015. A review on: CO2 capture technology on fossil fuel power plant. J. Fundam. Renew. Energy Appl. https://doi.org/10.4172/2090-4541.1000164.

Edwards, T.J., Maurer, G., Newman, J., Prausnitz, J.M., 1978. Vapor-liquid equilibria in multicomponent aqueous solutions of volatile weak electrolytes. AIChE J. https://doi.org/10.1002/aic.690240605.

Fang, M., Xiang, Q., Yu, C., Xia, Z., Zhou, X., Cai, D., Wang, Z., Yu, H., 2015. Experimental study on CO2 absorption by aqueous ammonia solution at elevated pressure to enhance CO2 absorption and suppress ammonia vaporization. Greenh. Gases Sci. Technol. https://doi.org/10.1002/ghg.1463.

Frank, M.J.W., Kuipers, J.A.M., Van Swaaij, W.P.M., 1996. Diffusion coefficients and viscosities of CO2 + H2O, CO2 + CH3OH, NH3 + H2O, and NH3 + CH3OH liquid mixtures. J. Chem. Eng. Data. https://doi.org/10.1021/je950157k.

Fu, Y., Bao, J., Singh, R., Wang, C., Xu, Z., 2020. Investigation of countercurrent flow profile and liquid holdup in random packed column with local CFD data. Chem. Eng. Sci. https://doi.org/10.1016/j.ces.2020.115693.

Kierzkowska-Pawlak, H., 2012. Determination of kinetics in gas-liquid reaction systems An Overview. Ecol. Chem. Eng. S 19, 175–196. https://doi.org/10.2478/v10216-011-0014-y.

Lawal, O., Bello, A., Idem, R., 2005. The role of methyl diethanolamine (MDEA) in preventing the oxidative degradation of CO2 loaded and concentrated aqueous monoethanolamine (MEA)-MDEA blends during CO2 absorption from flue gases. Ind. Eng. Chem. Res. https://doi.org/10.1021/ie049261y.

Li, K., Yu, H., Qi, G., Feron, P., Tade, M., Yu, J., Wang, S., 2015. Rate-based modelling of combined SO2 removal and NH3 recycling integrated with an aqueous NH3-based CO2 capture process. Appl. Energy. https://doi.org/10.1016/j.apenergy.2015.03.060.

Li, W., Zhao, X., Liu, B., Tang, Z., 2014. Mass transfer coefficients for CO2 absorption into aqueous ammonia using structured packing. Ind. Eng. Chem. Res. https://doi.org/10.1021/ie403097h.

Marshall, W.L., Franck, E.U., 1983. Ion product of water substance, 0–1000 °C, 1–10,000 bars new international formulation and its background. J. Phys. Chem. Ref. Data. Doi 10 (1063/1), 555643.

Niu, Z., Guo, Y., Zeng, Q., Lin, W., 2012. Experimental studies and rate-based process simulations of CO2 absorption with aqueous ammonia solutions. Ind. \& Eng. Chem. Res. 51, 5309–5319.

NOAA, National Centers for Environmental Information, 2023, 2023. Monthly Global Climate Report for Annual 2022. published online January 2023.
Ochedi, F.O., Yu, J., Yu, H., Liu, Y., Hussain, A., 2021. Carbon dioxide capture using liquid absorption methods: a review. Environ. Chem. Lett. https://doi.org/10.1007/s10311-020-01093-8.
Onda, K., Takeuchi, H., Okumoto, Y., 1968. Mass transfer coefficients between gas and liquid phases in packed columns. J. Chem. Eng. Japan. https://doi.org/10.1252/jcej.1.56.
Perrin, D.D., 1969. Dissociation contants of inorganic acids and bases in aqueous solution. Pure Appl. Chem. 20, 133–236.
Perry, R.H., Green, D.W., Maloney, J.O., 1999. Perry's chemical engineers' handbook, Seventh Edition. McGraw Hill.
Poling, B.E., Prausnitz, J.M., O'Connell, J.P., 2001. The Properties of Gases and Liquids, 5th Edition, Journal of the American Chemical Society.
Powlson, D.S., Dawson, C.J., 2022. Use of ammonium sulphate as a sulphur fertilizer: Implications for ammonia volatilization. Soil Use Manag. https://doi.org/10.1111/sum.12733.
Qi, G., Wang, S., Yu, H., Wardhaugh, L., Feron, P., Chen, C., 2013. Development of a rate-based model for CO2 absorption using aqueous NH3 in a packed column. Int. J. Greenh. Gas Control. https://doi.org/10.1016/j.ijggc.2013.05.027.
Qin, F., Wang, S., Hartono, A., Svendsen, H.F., Chen, C., 2010. Kinetics of CO2 absorption in aqueous ammonia solution. Int. J. Greenh. Gas Control 4, 729–738. https://doi.org/10.1016/j.ijggc.2010.04.010.
Ramesh, K., Aziz, N., Shukor, A., Ramasamy, M., 2007. Dynamic Rate-Based and Equilibrium Model Approaches for Continuous Tray Distillation Column. J. Appl. Sci. Res.
Rivera-Tinoco, R., Bouallou, C., 2010. Comparison of absorption rates and absorption capacity of ammonia solvents with MEA and MDEA aqueous blends for CO2 capture. J. Clean. Prod. https://doi.org/10.1016/j.jclepro.2009.12.006.
Rosenberg, R.M., Peticolas, W.L., 2004. Henry's law: A retrospective. J. Chem. Educ. https://doi.org/10.1021/ed081p1647.
Saidi, M., 2017. Mathematical modeling of CO2 absorption into reactive DEAB solution in packed columns using surface-renewal penetration theory. J. Taiwan Inst. Chem. Eng. https://doi.org/10.1016/j.jtice.2017.07.012.
Sander, R., 2015. Compilation of Henry's law constants (version 4.0) for water as solvent. Atmos. Chem. Phys. https://doi.org/10.5194/acp-15-4399-2015.
Seo, J.B., Jeon, S.B., Lee, S.S., Kim, J.Y., Oh, K.J., 2011. The physical solubilities and diffusivities of N2O and CO2 in aqueous ammonia solutions on the additions of AMP, glycerol and ethylene glycol. Korean J. Chem. Eng. https://doi.org/10.1007/s11814-011-0030-8.
Suess, P., Spiegel, L., 1992. Hold-up of mellapak structured packings. Chem. Eng. Process. https://doi.org/10.1016/0255-2701(92)85005-M.
van Swaaij, W.P.M., Versteeg, G.F., 1992. Mass transfer accompanied with complex reversible chemical reactions in gas-liquid systems: an overview. Chem. Eng. Sci. https://doi.org/10.1016/0009-2509(92)85028-A.
Versteeg, G.F., Van-Swaaij, W.P.M., 1988. Solubility and diffusivity of acid gases (CO2 and N2O) in aqueous alkanilamine solutions. J. Chem. Eng, Data.
Wang, F., Deng, S., Zhao, J., Yan, J., 2017. A novel ammonia-based CO2 capture process hybrid ammonia absorption refrigeration, in: Energy Procedia. https://doi.org/10.1016/j.egypro.2017.12.269.
Wang, G.Q., Yuan, X.G., Yu, K.T., 2005. Review of mass-transfer correlations for packed columns. Ind. Eng. Chem. Res. https://doi.org/10.1021/ie050017w.
Whitman, W.G., 1923. A Preliminary Experimental Confirmation of The two film theory of gas absorption. Chem. Metall, Eng.
Zeng, Q., Guo, Y., Niu, Z., Lin, W., 2013. The absorption rate of CO2 by aqueous ammonia in a packed column, in: Fuel Processing Technology. https://doi.org/10.1016/j.fuproc.2012.05.005.
Zhao, B., Su, Y., Tao, W., Li, L., Peng, Y., 2012. Post-combustion CO2 capture by aqueous ammonia: A state-of-the-art review. Int. J. Greenh. Gas Control. https://doi.org/10.1016/j.ijggc.2012.05.006.